



Repositorio Institucional de la Universidad Autónoma de Madrid

<https://repositorio.uam.es>

Esta es la **versión de autor** del artículo publicado en:
This is an **author produced version** of a paper published:

The Journal of Physical Chemistry B 122.11
(2018): 2975-2984

DOI: <https://doi.org/10.1021/acs.jpcb.7b12560>

Copyright: © 2018 American Chemical Society Publication

El acceso a la versión del editor puede requerir la suscripción del recurso
Access to the published version may require subscription

Solvent Effects on Electronically Excited States: QM/continuum vs QM/explicit models.

Martina De Vetta,^{a,b} Maximilian F. S. J. Menger,^{a,c} Juan J. Nogueira^{a,} and Leticia González^{a,*}*

a. Institute of Theoretical Chemistry, University of Vienna, Währinger Str. 17, A-1090 Wien, Austria

b. Departamento de Química, Universidad Autónoma de Madrid, c/ Francisco Tomás y Valiente 7, 28049 Cantoblanco, Madrid, Spain

c. Dipartimento di Chimica e Chimica Industriale, University of Pisa, Via G. Moruzzi 13, 56124 Pisa, Italy.

KEYWORDS: Electronically Excited States, Quantum Chemistry, Solvent Effects, Hydrogen Bonding, QM/MM, QM/PCM.

Corresponding Authors

Juan J. Nogueira: nogueira.perez.juanjose@univie.ac.at

Leticia González: leticia.gonzalez@univie.ac.at

ABSTRACT. The inclusion of solvent effects in the calculation of excited states is key to obtain reliable absorption spectra and density of states of solvated chromophores. Here we analyze the performance of three classical approaches to describe aqueous solvent in the calculation of the absorption spectra of pyridine, tropone and tropothione. Specifically, we compare the results obtained from quantum mechanics/polarizable continuum model (QM/PCM) versus quantum mechanics/molecular mechanics (QM/MM) in its electrostatic-embedding (QM/MMee) and polarizable-embedding (QM/MMpol) fashions, against full-QM computations, in which the solvent is described at the same level of theory as the chromophore. We show that QM/PCM provides the best results describing the excitation energies of $\pi\pi^*$ and $n\pi^*$ transitions of pyridine and tropone and $\pi\pi^*$ transitions of tropothione. However, accurate results for the $n\pi^*$ states of tropothione are obtained only when the PCM cavity is modified at the sulfur atom. The use of QM/MMee also provides accurate excitation energies for both $\pi\pi^*$ and $n\pi^*$ excitations, although they are slightly worse than those obtained from QM/PCM. The QM/MMpol approach performs as well as QM/PCM for describing the energy of $\pi\pi^*$ states but it is not able to provide a satisfactory description of hydrogen-bonding effects on the $n\pi^*$ states. The relative intensity of the absorption bands is better accounted for by the explicit-solvent models than by the continuum-solvent approach.

1. INTRODUCTION

The study of electronically excited-state processes is a continuous challenge for theory due to the many ingredients that need to be included to achieve experimental accuracy.^{1,2} One important component in the calculation is the inclusion of the environment.³ The environment can participate actively in the excitation process⁴⁻⁷ or passively, by only modifying the involved potential-energy surfaces or electronic properties of the chromophore.⁸⁻¹¹ In the latter case, when the electronic excitation is only localized in the chromophore, that is, when the electronic structure of the environment is barely affected by the excitation process, a classical description of the environment to obtain the excited states of the full system is typically employed.

One of the most common ways to describe solvent effects classically is the use of continuum models.¹²⁻¹⁵ Here, the apparent surface charge (ASC) methods, such as the polarizable continuum model (PCM)¹⁶ and the conductor-like screening model (COSMO),¹⁷ are the most popular ones. In many publications the term “continuum models” is used to refer exclusively to ASC methods, although that term is more general as other continuum models different from the ASC ones exist.^{18,19} In the present study, we will discuss only ASC methods and for convenience we will also employ the term “continuum model” as a synonymous of a “ASC model”. Under a continuum approach, the excited-state calculation is performed by using a QM/continuum partition of the system, in which the chromophore is described by a quantum mechanical (QM) method and the solvent by a dielectric or conductor continuum model. From the technical point of view, the ASC methods solve the Poisson equation in terms of a boundary element method. Accordingly, the chromophore is located into a cavity whose surface is divided into several small surface elements containing point charges.¹⁴ The charge distribution of the surface of the cavity is intended to reproduce the charge distribution of the solvent. The electrostatic interaction

between the chromophore and the solvent is represented by the interaction between the electrostatic potential created by the chromophore and the charge distribution of the cavity surface. Such an interaction is computed self-consistently so that the chromophore and the solvent are mutually polarized. Excited-state calculations employing a QM/continuum scheme have been performed for a countless number of chromophores (see for example Ref. 20) because nowadays continuum models are very efficiently implemented in many quantum-chemistry packages in a black-box fashion, despite their high complexity. In addition, since continuum models describe the solvent degrees of freedom in an average way, configurational sampling of the solvent is not needed. Therefore, the calculation of, e.g., the absorption spectrum of a chromophore requires only one single-point calculation employing, usually, the ground-state minimum-energy geometry of the chromophore.

An alternative mainstream method to describe solvent effects is the use of quantum mechanics/molecular mechanics (QM/MM) schemes,^{21,22} in which the solvent is explicitly described by a MM force field while the QM region comprises the chromophore. The accuracy of QM/MM calculations largely relies on the complexity chosen to describe the interactions between the QM and MM regions. In the simplest approach, the so-called QM/MM mechanical embedding, this interaction is computed classically by a force field. However, a vertical-energy calculation using the mechanical embedding is equivalent to a gas-phase calculation because force fields are usually parameterized for the ground state and the same parameter values are used for the excited states. Accordingly, the classical energy terms cancel out when the vertical energy is obtained as the energy difference between the states involved in the excitation. A more adequate description is obtained by the QM/MM electrostatic embedding (QM/MMee), in which the MM fixed charges of the solvent are introduced in the Hamiltonian of the chromophore so

that the electronic structure of the chromophore is polarized by the charge distribution of the solvent. A better description is achieved in the QM/MM polarizable embedding schemes by introducing a mutual polarization between the chromophore and the solvent, where the use of polarizable force fields allows the solvent to modify its charge distribution. One way to include polarization in the solvent is to make use of induced dipoles, as it is done in the QM/MMpol approach.²³ Regardless of the embedding scheme, a large number of solvent molecules are explicitly included in all QM/MM approaches. This means that many possible solvent configurations are energetically accessible and, thus, the configurational space needs to be sampled efficiently. This is usually done by evolving classical or QM/MM molecular dynamics (MD) simulations³ in advance. After the sampling process is completed, the excited states of the chromophore are then computed for a sufficiently large number of snapshots. As configurational sampling followed by multiple QM/MM excited-state calculations is less straightforward and, usually, more expensive than a geometry optimization followed by a single-point QM/continuum calculation, QM/MM methods are less extended than QM/continuum methods for excited states.

When a chromophore is embedded in solvent the chromophore/solvent interactions can be classified in two types: (i) interactions between the chromophore and the bulk solvation and (ii) interactions between the chromophore and specific groups of the solvent, e.g., hydrogen bonding or stacking.²⁴ In polar solvents, e.g., water, electrostatic interactions largely dominates both the interactions with bulk solvation and specific interactions. Electrostatic interactions with bulk solvation can induce red- or blue-shifts in the absorption bands of the chromophore, depending on the excited-state and the ground-state dipole moments (see Figure 1a): if the dipole moment of a particular excited state is larger than the dipole moment of the ground state, the excited state is energetically stabilized with respect to the ground state when the chromophore goes from the

gas phase to solvent. As a consequence, the vertical energy of that excited state is red shifted upon solvation. Contrary, when the dipole moment of the excited state is smaller than that of the ground state, the excitation is blue shifted because the energy of the excited state increases with respect to the ground-state energy. All the QM/classical models mentioned above are able to properly describe interactions with bulk solvation. However, QM/continuum and QM/MM polarizable-embedding models should provide better results than QM/MM electrostatic-embedding models since in the former approaches the chromophore/solvent interactions are computed in a self-consistent manner.

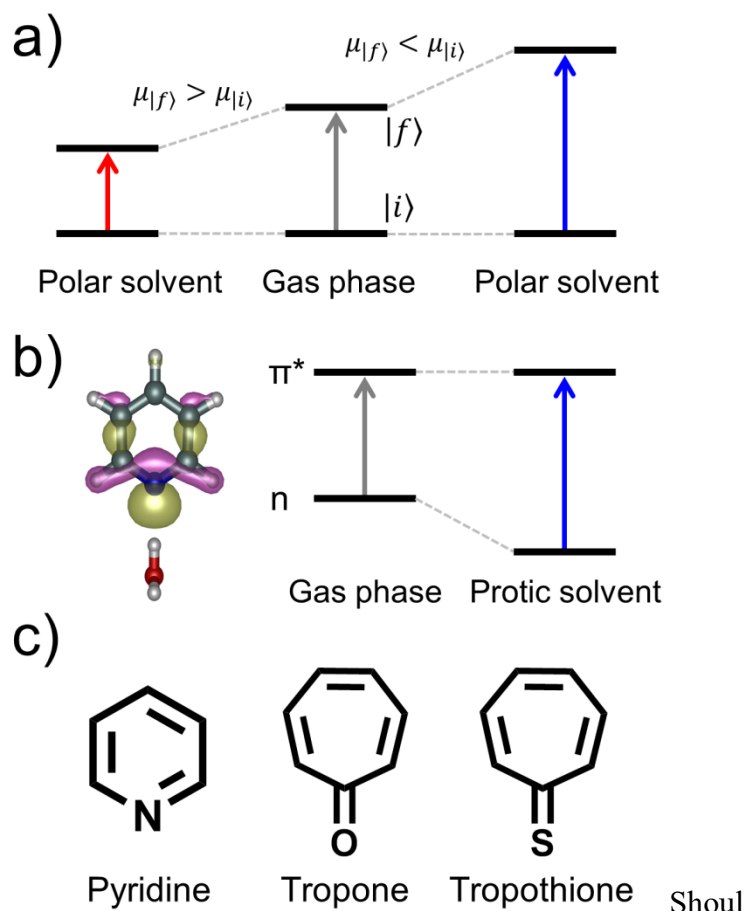


Figure 1. (a) Schematic representation of the red (left) or blue (right) shift of an electronic transition depending on the relation between the dipole moments of the ground ($\mu_{|i\rangle}$) and excited

($\mu_{|i\rangle}$) states. (b) Non-bonding orbital of pyridine centered at the N atom and schematic representation of the blue-shift of an electronic $n\pi^*$ transition induced by hydrogen bonding. Color code for atoms: N in blue, C in grey, O in red, and H in white. (c) Chromophores theoretically investigated here: pyridine, tropone, and tropothione.

In protic solvents, the most common specific interaction is hydrogen bonding, especially when the chromophore possesses a heteroatom in its structure. Hydrogen bonding may induce important energy shifts in the excited states in which heteroatoms are involved. This is the case of $n\pi^*$ electronic transitions (see Figure 1b), with the nonbonding orbital n centered in the heteroatom. The hydrogen bond stabilizes the n orbital and the energy gap between that orbital and the π^* orbital increases, resulting in a blue-shift of the excitation energy. This was, for example, the case in methylene blue, when comparing its excited states in aqueous solution against those of the chromophore embedded in a lipid bilayer⁸ or intercalated in a DNA double strand.⁹ In general, it is stated that continuum models are not able to describe the effect of hydrogen bonding and, thus, an explicit description of the solvent, like in QM/MM schemes, is necessary.^{3,25-28} However, both QM/MM and QM/continuum approaches are more similar than it might seem at first glance since in both methodologies the solvent is described by a distribution of charges that polarizes the electronic-structure of the chromophore. In addition, as it was pointed out by Tomasi,²⁹ the hydrogen-bond energy is well described by electrostatic, exchange and dispersion terms used in continuum models. Therefore, there is no reason to think that QM/MM models will perform much better than QM/continuum models, even when hydrogen-bond interactions are present in the system. Nevertheless, one should not forget that even if classical models (both continuum and explicit approaches) can provide a good description of hydrogen-bonding effects, they are not capable of describing the hydrogen bond itself because,

besides the electrostatic interactions that are well described by classical models, hydrogen bonds also present quantum features. For example, it is well known that an important energetic contribution to the hydrogen-bond energy is associated to charge transfer.³⁰ This charge transfer mainly involves electron transfer from the lone pair of the hydrogen-acceptor heteroatom to the sigma antibonding orbital in which the hydrogen atom is involved. Since classical models do not explicitly describe the electronic structure of the solvent, this electron transfer from the chromophore to the solvent or *vice versa* is missing.

In this paper, we want to challenge several QM/classical schemes, namely QM/continuum, QM/MMee, and QM/MMpol to describe the effect of bulk solvation and hydrogen bonding on systems possessing a heteroatom and therefore forming hydrogen bonds with water molecules. Specifically, we shall examine the electronically excited states of the chromophores pyridine, tropone and tropothione (Figure 1c). The deficiencies and strengths of the three classical approaches will be discussed by comparison of full quantum mechanical calculations, which consider explicit solvent molecules at the same quantum mechanical level as the chromophore, with the results of the three QM/continuum models chosen.

2. COMPUTATIONAL METHODS

2.1 Gas-phase Excited-State Calculations

As the main goal of this work is to investigate solvent effects on the electronically excited states of different chromophores, the first step is to compute the excitation energies of the chromophores in the gas phase. All quantum mechanical calculations were performed by the Gaussian09 package.³¹ The ground-state geometry of pyridine, tropone and tropothione was optimized in the gas phase at density-functional theory (DFT) level using the CAM-B3LYP

functional³² and the 6-31+G* basis set. Then, the excitation energies of the eight lowest-energy states were computed by time-dependent DFT (TD-DFT) with the same functional and basis set. Note that our goal is to compare the excitation energies of different QM/classical schemes and not to obtain the most accurate description of the excited states. Therefore, we have employed a reasonable level of theory but without benchmarking it by comparison with higher-level calculations or experiment.

2.2 QM/PCM Excited-State Calculations

In the second step, the vertical-excitation energies of the eight lowest-energy states are computed in water by using the integral-equation formalism of the polarizable-continuum model (IEF-PCM)¹⁴ to describe the solvent. The linear response (LR) formulation of PCM/TD-DFT was employed, in which the excitation energies are directly computed.³³ The calculation of the excitation energies were performed in the non-equilibrium regime, in which the electronic (fast) degrees of freedom of the solvent are in equilibrium with the excited-state electronic density of the chromophore, while the nuclear (slow) degrees of freedom of the solvent are in equilibrium with the ground-state electronic density of the chromophore. The slow and fast responses of the solvent are governed by the static dielectric constant ϵ and the dielectric constant at optical frequency ϵ_{opt} , respectively.¹⁴ The default values for water of 78.353 for ϵ and 1.778 for ϵ_{opt} were used. An additional parameter that is necessary to choose in PCM calculations is the atomic radii, which define the cavity surface where the charges of the solvent that interact with the solute are located. It has been shown that excitation energies are very sensitive to the cavity size.³⁴ Two different set of radii, namely Universal Force Field (UFF) and Bondi radii, were employed to investigate the effect of the size of the cavity on the excitation energies of the chromophores. UFF radii (default radii in Gaussian09) are larger than the Bondi ones;

specifically, the Bondi radii for the C, N, O, S and H atoms are 1.70, 1.55, 1.52, 1.80 and 1.20 Å and the UFF values are 1.92, 1.83, 1.75, 2.02 and 1.44 Å. As can be seen, the radius values differ significantly and, thus, a large impact on the excitation energies might be expected. Moreover, additional values for the S atom were used in the excited-state calculations for tropothione. This will be discussed in more detail in Section 3. When solving the electrostatic equations in the PCM procedure, the cavity is scaled by an empirical factor α . The default value in Gaussian09 of 1.1 was used for both set of radii. In order to investigate solely solvent effects on the excitation energies when comparing gas-phase with QM/PCM calculations, the gas-phase optimized geometry was used for the PCM computations. In this way, energy shifts induced by geometrical modifications of the chromophore are removed and a direct analysis on solvent effects is possible.

2.3 QM/MMee and QM/MMpol Excited-State Calculations

The excitation energies were also computed using the QM/MMee and QM/MMpol schemes. In these two approaches explicit solvent molecules are introduced in the model, while the PCM method considers the solvent degrees of freedom in an average way. In order to compare the results from QM/MM with the ones from QM/PCM, the position of the water molecules in the explicit models needs to be efficiently sampled to obtain also an average picture of the solvent and not only one or few arbitrary solvent geometrical configurations. The solvent degrees of freedom were sampled by running classical MD simulations. First, the gas-phase optimized geometries of pyridine, tropone and tropothione were solvated by a periodic truncated octahedral box of water molecules extended to a distance of 14 Å from any solute atom by the leap module of AmberTools17.³⁵ Then, the solvated chromophores were heated to 300 K at constant volume (NVT), using the Berendsen thermostat with a time constant for the bath coupling of 0.5 ps⁻¹, for

50 ps with a time step of 1 fs. Once the system was at 300 K, the density of the solvent was equilibrated at constant pressure (NPT) during a 2 ns simulation with a time step of 2 fs. The Berendsen barostat with a pressure relaxation time of 2 ps was used to maintain a pressure of 1 bar. The Coulomb and van der Waals interactions were truncated at 10 Å and the particle mesh Ewald method³⁶ was employed to calculate the Coulomb interactions. The bond distances involving H atoms were restrained by the SHAKE algorithm.³⁷ The chromophores were described by the General Amber Force Field (GAFF) for organic molecules³⁸ and the water molecules by the TIP3P force field.³⁹ The geometry of the chromophores was frozen during the MD simulations, so that alterations in the excitation energies due to the vibrational motion of the chromophore are eliminated and, thus, the comparison between the QM/MM and QM/PCM schemes provides energy differences that are exclusively caused by the use of different solvent models. All classical MD simulations were performed using the sander module implemented in the Amber16 program.³⁵

Once the thermal MD ensembles are obtained, 100 equidistant snapshots from the last 1 ns of the trajectories are selected for each chromophore. Then, the eight lowest-lying electronically excited states for each of the 100 snapshots for the three chromophores are computed by the QM/MM_{ee} and QM/MM_{pol} schemes. The chromophores are included in the QM region and described at the same level of theory as in the gas-phase and QM/PCM excited-state calculations. In the QM/MM_{ee} scheme the atomic point charges of the water molecules are included in the Hamiltonian of the QM region. This means that the charges of the solvent, which were taken from the TIP3P force field, polarize the electronic density of the chromophore but the solvent does not respond to the changes in the electronic structure of the chromophore. In the QM/MM_{pol} scheme not only the QM region is polarized by the MM region but also the MM

region is polarized by the QM region. Such a mutual polarization is described here by using the QM/MMpol approach developed by Mennucci and coworkers.^{23,40} In this approach, in addition to the electrostatic interaction between the fixed charges of the environment and the electronic density of the chromophore which is also present in QM/MMee, there is also interaction between induced dipole moments of the MM region and the electric field produced by the QM region. Since the induced dipole moments of the MM region depend on the electric field of the QM region and *vice versa*, the computation of the mutual polarization is performed in a self-consistent manner. These calculations employed the isotropic polarizabilities of Wang *et al.*^{41,42} to compute the induced dipoles; the point charges were taken from Ref. 43, where they have been computed at MP2/ 6-311++G(d,p) level of theory for the TIP3P geometry. The QM/MMpol calculations were run by a development version of Gaussian09.³¹

In order to obtain the absorption spectra of the three chromophores, the resulting excitation energies for the 100 geometries were convoluted with Gaussian functions with full width at half maximum of 0.20 eV. The heights of the Gaussian functions are proportional to the oscillator strengths of the electronically excited states. Then, the most intense band is scaled to unity and the other bands are scaled by the same factor. In addition, we have also computed the density of states (DOS) for the electronic states dominated by $n\pi^*$ transitions, which are the states that present a larger shift due to hydrogen bonding. As we have computed eight excited states for 100 geometries for each of the three chromophores, it means a total of 2400 states to analyze in order to identify the $n\pi^*$ states. This has been done automatically using the electronic transition density within the TheoDORÉ package.⁴⁴⁻⁴⁶ Specifically, the two lowest-energy states dominated by $n\pi^*$ transitions were identified as the two states with the largest hole population at the heteroatom (N for pyridine, O for tropone and S for tropothione). Then, the DOS were obtained by convoluting

the energies of $n\pi^*$ states with Gaussian functions with full width at half maximum of 0.20 eV and height equal to unity.

2.4 Full-QM Excited-State Calculations

As a benchmark, a more accurate model describing the solvent molecules than the different QM/classical schemes is required. An obvious choice would be to describe the solvent molecules at the same level of theory as the chromophore. However, as the investigated systems contain around 1000 water molecules, it is computational unfeasible to treat all of them at TD-DFT level for 100 geometries. Instead, we have selected a smaller amount of solvent molecules to calculate the absorption spectra and the DOS. The number of solvent molecules needed to obtain converged excited-state energies was selected using the following procedure. First, for each solvated chromophore, two different snapshots were chosen: one where the chromophore undergoes hydrogen bonding with one solvent molecule and one without. We consider a hydrogen bond formed when the separation between the hydrogen acceptor (the heteroatom of the chromophore) and the hydrogen donor (the O atom of water) is smaller than 3.5 Å and the angle formed by the hydrogen donor, hydrogen atom, and hydrogen acceptor is larger than 135°. The hydrogen-bond analysis was performed by the CPPTRAJ program.⁴⁷ Then, for each of the two snapshots the eight lowest-energy excited states were computed by including the N closest water molecules while the remaining water molecules were removed. For pyridine and tropone N goes from 0 (gas phase) to 70, and for tropothione it goes from 0 to 100. Figure 2 displays the energy variation of the brightest $\pi\pi^*$ state and the two lowest $n\pi^*$ states with N . The involved π and n orbitals are shown in Figure 3. As can be seen, the excitation energies of the three investigated states exhibit strong oscillations for small N , but they are converged after including 40 water molecules for pyridine and tropone and 80 water molecules for tropothione.

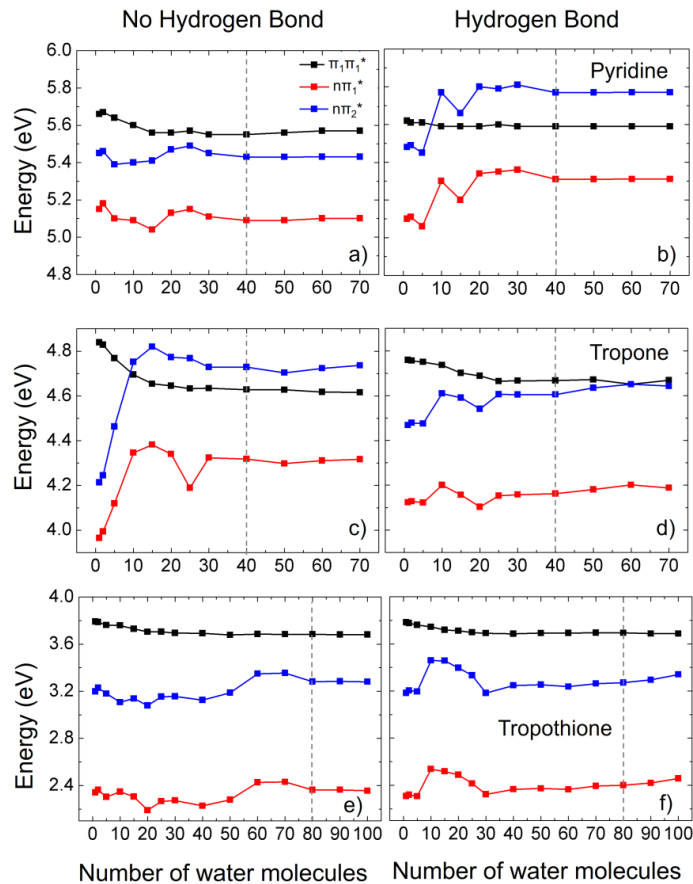


Figure 2. Variation of the excited-state energies of the brightest $\pi\pi^*$ state and the two lowest-energy $n\pi^*$ states with the number of water molecules described at the same level of theory as the chromophores: pyridine (a, b), tropone (c, d), and tropothione (e, f). Two different snapshots are considered, one that presents hydrogen bonding between the chromophore and solvent (a, c, e) and another that does not (b, d, f). The involved π and n orbitals are shown in Figure 3.

Accordingly, the same 100 snapshots employed for the QM/MM calculations were selected and for each, the eight lowest-energy states were computed including the closest 40 water molecules for pyridine and tropone, and the closest 80 water molecules for tropothione. The remaining water molecules were removed from the system. Hereinafter, we shall refer to this approach as the full-QM approach. The absorption spectrum and the DOS for the $n\pi^*$ states were obtained by

convoluting the excitation energies as explained in Section 2.3. For a few particular geometries, we noticed that charge-transfer states, in which an electron is transferred from the chromophore to the solvent, lie low in energy. This is not surprising considering that TD-DFT usually underestimates the energy of charge-transfer states, even with a range-separated functional, as the one used here.⁴⁸ It is not the scope of this study to investigate whether the energies of these charge-transfer states are accurate or whether they are underestimated by the functional. Since the classical QM/PCM and QM/MM approaches that we shall compare below are not able to describe charge-transfer states, they have not been considered in the convolution of the excitation energies to obtain the full-QM absorption spectra and DOS. In order to identify the charge-transfer states, each system is divided in two fragments: the chromophore and the solvent. Then, the charge-transfer number between fragments, which provides the fraction of electron that is transferred between the chromophore and the solvent, is computed from the transition density matrix using the TheoDORE package.⁴⁴⁻⁴⁶ Those states whose charge-transfer number is larger than 0.2 were not considered in the analysis.

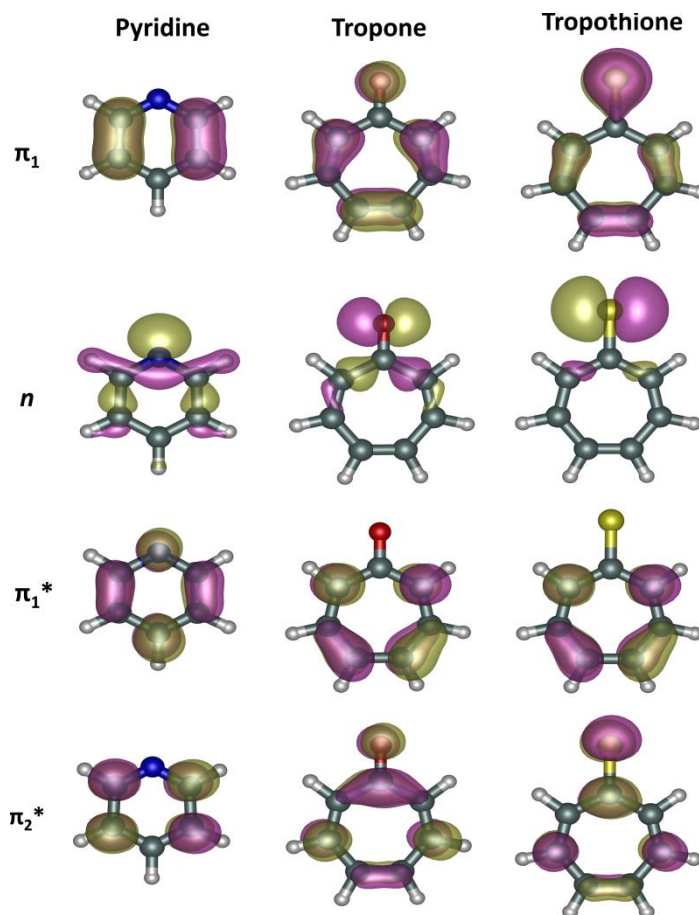


Figure 3. Orbitals involved in the brightest $\pi\pi^*$ electronic state and in the two lowest-energy $n\pi^*$ states of pyridine, tropone, and troprothione.

3. RESULTS AND DISCUSSION

In this section the excited-state calculations for pyridine, tropone and troprothione performed in the gas phase and with the different solvent models will be analyzed. First, solvation effects on the excitation energies will be discussed based on the comparison between the gas-phase vertical energies and the full-QM absorption and DOS bands. Second, the QM/PCM vertical energies will be compared with the full-QM bands to investigate the performance of the continuum approach. In addition, the consequences of using several atomic radius values in PCM will be

evaluated. Then, the explicit solvation models, namely QM/MM_{ee} and QM/MM_{pol}, will be compared with the full-QM and QM/PCM results. This comparison will allow us to discuss whether the introduction of explicit water molecules and thermal sampling improves the results with respect to the average solvent configuration provided by PCM. Finally, the comparison between the QM/MM_{ee} and QM/MM_{pol} bands will reveal the importance of including polarization in the solvent. The analyses will be performed for the absorption spectra (bright $\pi\pi^*$ transitions) in Section 3.1 and for the DOS for $n\pi^*$ transitions in Section 3.2.

3.1 Absorption Spectrum

Gas-phase and QM/PCM vertical energies together with the full-QM, QM/MM_{ee} and QM/MM_{pol} absorption spectra are plotted in Figure 4 for the three chromophores and energies at the absorption maxima and the absolute (unsigned) errors with respect to the full-QM computations are listed in Table 1. When comparing the gas-phase vertical energies with the full-QM absorption bands one can see that for pyridine (Figure 4a) and tropothione (Figure 4d) the bands are red-shifted when going from the gas phase to solvent. The red-shift is 0.09 eV for both bands of pyridine and 0.13 eV for the absorption band of tropothione. As discussed in Section 1, based only on simple electrostatic-interaction criteria, the red-shift of the bands would be a consequence of the larger dipole moments of the excited states with respect to that of the ground state. Indeed, the dipole moments of the bright states involved in bands 1 and 2 of pyridine are 2.15 and 2.54 D, respectively, while it is 2.41 D for the ground state; in tropothione, the excited-state and ground-state dipole moments are 6.26 and 5.48 D, respectively. Therefore, the simple electrostatic model is able to explain the red-shift of band 2 of pyridine and the band of tropothione. However, it predicts an erroneous blue-shift for the band 1 of pyridine. Understanding the energy behavior of this band requires a more complex analysis. The $\pi_1\pi_1^*$

transition (see orbitals in Figure 3) represents the largest contribution to band 1 of pyridine. As can be seen, the π_1^* molecular orbital has important contributions from atomic orbitals centered at the N atom. Therefore, when pyridine undergoes hydrogen bonding with the solvent, the π_1^* is stabilized and the $\pi_1\pi_1^*$ transition is red-shifted. This is confirmed by decomposing the absorption spectrum into one band coming from MD snapshots where hydrogen bonding is present and another band computed from the snapshots that do not present hydrogen bonding, see Figure 4b. The total absorption band is completely dominated by the contribution coming from snapshots that present hydrogen bonding because actually, pyridine undergoes hydrogen bonding during 92% of the simulation time. The absorption band of pyridine is red-shifted by 0.05 eV when hydrogen bond is present in comparison with the band with no hydrogen bonding. Therefore, although the dipole moment of the $\pi_1\pi_1^*$ state (2.15 D) is smaller than the ground state dipole moment (2.41 D), the band is red-shifted when going from the gas phase to solution. For tropone, Figure 4b and Table 1 show that band 1 is blue-shifted (0.17 eV) and band 2 is red-shifted (0.18 eV) in solvent with respect to the gas phase. In that case, simple electrostatic considerations also explain the energy shifts: the main bright states contributing to bands 1 and 2 have dipole moments of 3.35 and 5.52 D, while the ground-state dipole moment is 4.88 D.

From the energy values of all the classical approaches compared with the full-QM energies in Table 1, the first general conclusion is that all classical models reproduce correctly the direction of the band shifts when going from the gas phase to solvation. In the following, each of the models will be examined in detail. We commence the discussion with the QM/PCM vertical energies. As can be seen in Table 1 and Figure 4, PCM provides very good results for the three chromophores with errors ranging from 0.02 to 0.09 eV. For pyridine and tropone the results obtained with the Bondi radii (errors around 0.02-0.03 eV) are slightly better than the results

obtained with the UFF radii (errors around 0.05-0.06 eV), which is the default radii in Gaussian09. Remarkable is that PCM reproduces very well band 1 of pyridine, despite the presence of important hydrogen-bonding effects, as explained above. Figures 4a,c show that the relative intensity between the two absorption bands in pyridine and tropone is also relatively well reproduced by QM/PCM, although the intensity of the less intense band is slightly overestimated with respect to the full-QM result.

In the case of tropothione, the accuracy of the vertical energy computed in PCM is reasonably accurate presenting an error of 0.04 and 0.06 eV when the UFF and Bondi radii are employed. This means that, contrary to what happens for pyridine and tropone, the use of UFF radii provides slightly better results. We find interesting to analyze this situation in more detail. The only difference in the atomic composition of the three chromophores investigated here is the heteroatom. The heteroatom in tropothione is the S atom, whose UFF and Bondi radii are 2.02 and 1.80 Å, respectively. Therefore, it seems that the use of larger radius for S provides better results. In this spirit, we have performed several QM/PCM excited-state calculations for tropothione with different increasing values of the S radius. The better agreement between the QM/PCM and the full-QM absorption spectra, which is the only result shown in Figure 4d and Table 1 for simplicity, was achieved for a radius value of 3 Å. The vertical energies obtained with other radius values will be discussed in Section 3.2 and it will be shown that the value of 3 Å also improves very much the DOS for the $n\pi^*$ transitions.

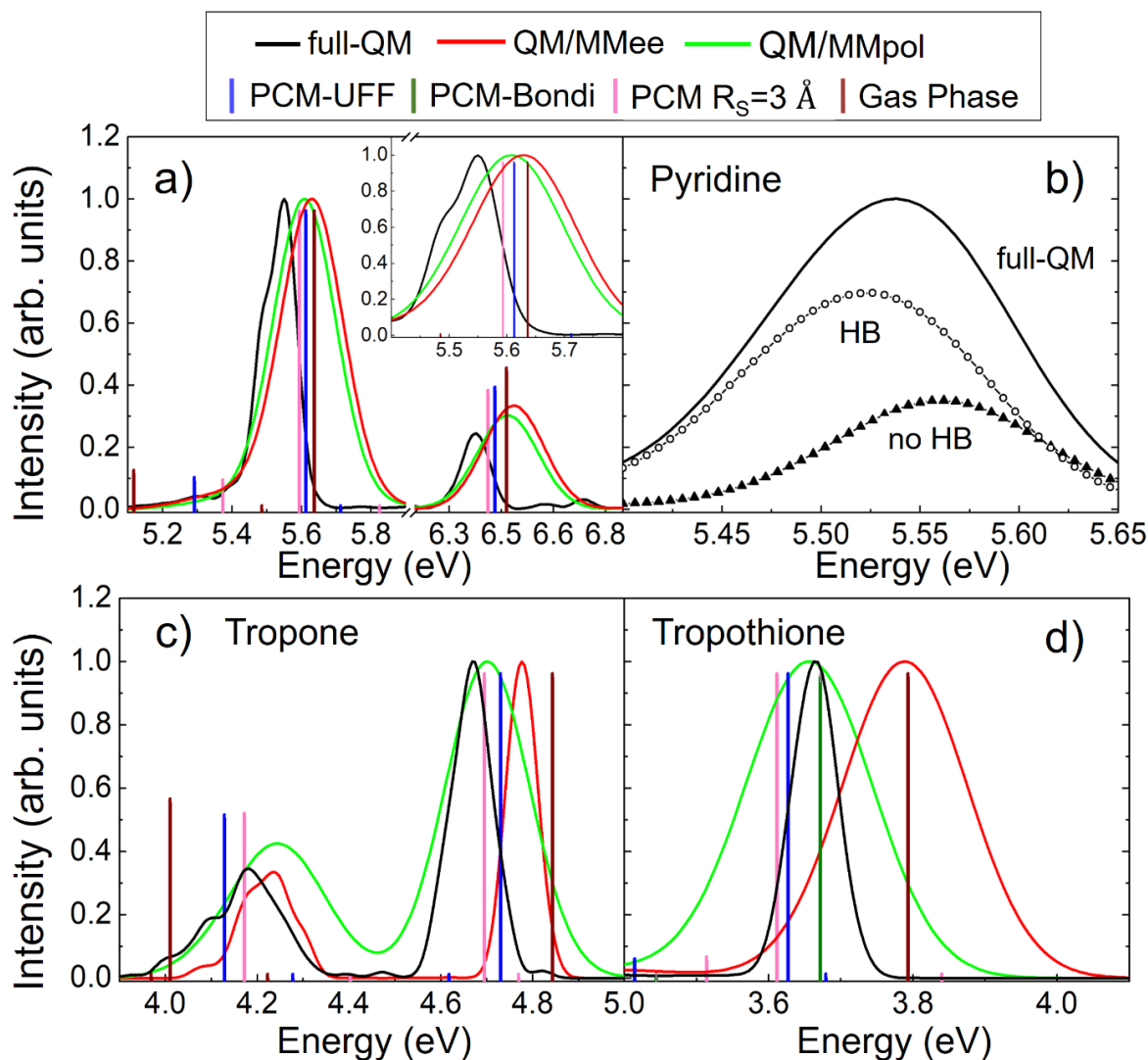


Figure 4. Vertical energies in the gas phase, vertical energies in water computed by the QM/PCM approach, and absorption spectra in water computed by the full-QM, QM/MMee, and QM/MMpol approaches for pyridine with an inset zooming the first absorption feature (a), tropone (c) and tropothione (d). Two different atomic radii, namely Universal Force Field (UFF) and Bondi radii, were used in the QM/PCM computations. A radius of 3 Å was also employed for the S atom of tropothione combined with UFF radii for the remaining atoms of the molecule. Panel (b) shows the absorption spectrum of pyridine decomposed into a contribution computed from snapshots that present hydrogen bonding (HB) and no hydrogen bonding (no HB).

Table 1. Vertical energies (in eV) in the gas phase, in water computed by the QM/PCM approach and energy at the absorption maxima of the spectra in water computed by the full-QM, QM/MMee, and QM/MMpol approaches for pyridine, tropone, and tropothione. Absolute errors with respect to the full-QM maxima are given in parenthesis.

		Gas	Full-QM	PCM (UFF ^a)	PCM (Bondi ^b)	QM/MMee	QM/MMpol
Pyridine	Band 1	5.64	5.55	5.61 (0.06)	5.59 (0.04)	5.63 (0.08)	5.6 (0.05)
	Band 2	6.47	6.38	6.43 (0.05)	6.41 (0.03)	6.49 (0.11)	6.47 (0.09)
Tropone	Band 1	4.01	4.18	4.13 (0.05)	4.17 (0.01)	4.24 (0.06)	4.24 (0.06)
	Band 2	4.84	4.66	4.73 (0.07)	4.70 (0.04)	4.78 (0.12)	4.7 (0.04)
Tropothione	Band 1	3.80	3.67	3.63 (0.04) 3.67 (0.00) ^c	3.61 (0.06)	3.79 (0.12)	3.65 (0.02)

^aUniversal Force Field (UFF) radii were employed in the QM/PCM computation.

^bBondi radii were employed in the QM/PCM computation.

^cQM/PCM vertical energy computed when a radius of 3 Å is used for S, while the UFF radii are used for the rest of the atoms.

Next, we examine the absorption spectra obtained by the QM/MMee approach. In general, the QM/MMee spectra agree well with the full-QM spectra although the energy errors are around 0.05-0.10 eV larger than the QM/PCM errors for any of the two radii. Again, it is interesting to focus on band 1 of pyridine, which is largely influenced by hydrogen bonding. As can be seen in Table 1, the QM/MMee error for this band is 0.08 eV, while it is 0.06 and 0.03 eV for QM/PCM using the UFF and Bondi radii, respectively. This means that QM/PCM reproduces better the red-shift of the band induced by hydrogen bonding than QM/MMee does. Overall, it seems that the mutual polarization between the chromophore and the solvent, which is taken into account in QM/PCM, is more important than the introduction of explicit solvent molecules and thermal sampling to obtain accurate energies. However, the QM/MMee approach describes better the

relative intensity of the absorption bands, as seen in Figures 4a,c. This indicates that the introduction of thermal sampling in the theoretical model is important to obtain a good description of the absorption intensities.

Finally, we discuss the accuracy of the QM/MMpol scheme, in which both mutual polarization between the chromophore and solvent and thermal sampling are considered. As it is shown in Figure 4 and Table 1, the QM/MMpol performs better than QM/MMee but worse than QM/PCM regarding the energy position of the bands, with errors between 0.02 and 0.09 eV. In addition, the relative intensity of the bands are reproduced with the same quality as those computed with QM/MMee. Therefore, considering both energies and intensities, QM/MMpol provides the most accurate results among the three QM/classical models. This is not surprising considering that the QM/MMpol approach combines the best features of the QM/PCM and QM/MMee methods.

3.2 Density of States for $n\pi^*$ Transitions

In the present section the solvent effect on the excitation energies of the electronically excited states dominated by $n\pi^*$ transitions is examined. As discussed above, it is expected that these states present strong energy blue-shifts upon solvation in protic solvents due to the participation of the heteroatom, which is very prone to form hydrogen bonds, in the hole-orbital involved in the electronic transition. Indeed, this is the case for the three chromophores investigated here, as can be seen in the DOS bands plotted in Figure 5 and the vertical energies and energies at the band maxima listed in Table 2. The comparison between the gas-phase vertical energies and the DOS in water computed by the full-QM approach shows very strong blue-shifts when going from the gas phase to solvent. Specifically, the blue shifts of the two $n\pi^*$ states are, in increasing order, 0.18 and 0.26 eV for tropothione, 0.27 and 0.30 for pyridine, and 0.32 and 0.42 for

tropone. The magnitude of the energy blue-shift is in consonance with the hydrogen bond ability of the heteroatom of the chromophore, i.e., S (tropothione) < N (pyridine) < O (tropone).

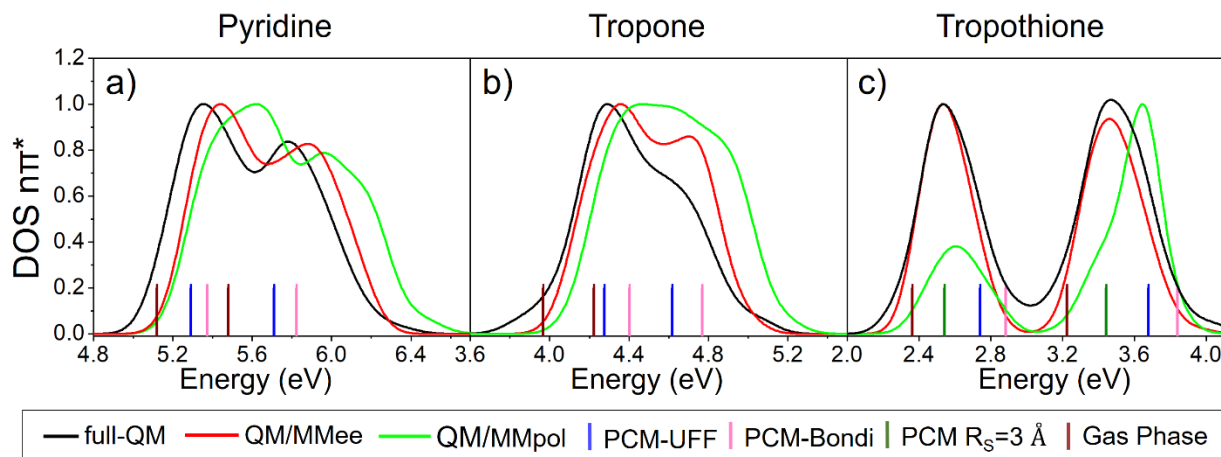


Figure 5. Vertical energies of the two lowest-energy $n\pi^*$ states in gas phase, in water using the QM/PCM approach, and density of states (DOS) for $n\pi^*$ states in water computed by the full-QM, QM/MMee, and QM/MMpol approaches for pyridine (a), tropone (b) and tropothione (c). Two different atomic radii, namely Universal Force Field (UFF) and Bondi radii, were used in the QM/PCM computations. Additionally, for tropothione a radius of 3 Å was employed for the S atom combined with UFF radii for the remaining atoms of the molecule.

The QM/PCM approach using the UFF and Bondi radii reproduces very well the hydrogen-bond-induced blue-shift for pyridine and tropone. For pyridine, the use of Bondi radii provides smaller errors (0.02 and 0.04 eV) than the use of UFF radii (0.06 and 0.08 eV). However, the opposite is found for the excitation energies of tropone, whose errors are 0.01 and 0.03 eV for UFF radii and 0.11 and 0.13 for Bondi radii. In the case of the absorption spectra, which is dominated by $\pi\pi^*$ transitions, it has been shown in Section 3.1 that the Bondi radii performs better than the UFF radii for both pyridine and tropone. This result is discouraging, although somehow expected,

since it implies that the accuracy of a particular set of radii depends on the chromophore and the electronic configuration of the excited states. For example, for tropone, the error of the QM/PCM vertical energy for the brightest state (band 1 in Table 1) using the Bondi radii is only 0.01 eV, while it amounts to 0.11 eV for the band 1 of the $\pi\pi^*$ DOS, i.e., the errors differ by one order of magnitude. Nevertheless, it is fair to conclude that the QM/PCM approach provides very good results for the $\pi\pi^*$ DOS of pyridine and tropone, which are strongly influenced by hydrogen bonding.

Table 2. Vertical energies (in eV) in the gas phase, in water computed by the QM/PCM approach and energy at the absorption maxima of the spectra in water computed by the full-QM, QM/MMee, and QM/MMpol approaches for pyridine, tropone, and tropothione. Absolute errors with respect to the full-QM maxima are given in parenthesis.

		GAS	Full-QM	PCM (UFF ^a)	PCM (Bondi ^b)	QM/MMee	QM/MMpol
Pyridine	Band 1	5.12	5.35	5.29 (0.06)	5.37 (0.02)	5.44 (0.09)	5.61 (0.26)
	Band 2	5.48	5.78	5.70 (0.08)	5.82 (0.04)	5.89 (0.11)	5.97 (0.19)
Tropone	Band 1	3.97	4.29	4.28 (0.01)	4.40 (0.11)	4.36 (0.07)	4.48 (0.19)
	Band 2	4.22	4.64	4.61 (0.03)	4.77 (0.13)	4.71 (0.07)	4.86 (0.22)
Tropothione	Band 1	2.36	2.54	2.75 (0.21) 2.54 (0.00) ^c	2.88 (0.34)	2.54 (0.00)	2.6 (0.06)
	Band 2	3.22	3.48	3.68 (0.20) 3.44 (0.04) ^c	3.84 (0.36)	3.46 (0.02)	3.65 (0.17)

^aUniversal Force Field (UFF) radii were employed in the QM/PCM computation.

^bBondi radii were employed in the QM/PCM computation.

^cQM/PCM vertical energy computed when a radius of 3 Å is used for S, while the UFF radii are used for the rest of the atoms.

The situation is completely different for the QM/PCM vertical energies of tropothione. As it is shown in Figure 5c and Table 2, the errors of the PCM computation are very large: 0.21 and 0.20 using the UFF radii and 0.34 and 0.36 using the Bondi radii. The accuracy of the $n\pi^*$ electronic states largely depends on the parameterization of the heteroatom, which in the case of tropothione is the S atom. In general, S atoms are not frequently present in organic and biological chromophores; therefore, its parameterization is, likely, not as much tested as the one for the N or O atoms. We have discussed in Section 3.1 that QM/PCM calculations have also been performed using several values for the S radius, while the UFF radii was used for the other atoms of tropothione. In the case of the brightest state, the best agreement with the full-QM absorption band was achieved for a radius value of 3 Å (see Table 1), for which the error is negligible. We have also used the same S radius for computing the $n\pi^*$ vertical energies and the results are shown in Figure 5c and Table 2. The error of the two $n\pi^*$ electronic states dramatically decreases from 0.21 and 0.20 eV when using the UFF radii to 0.00 and 0.04 eV when using a radius of 3 Å for the S atom. In Figure 6a we show the QM/PCM excitation energies using different values for the S atom ranging from the Bondi radius (1.80 Å) to 3 Å. The energy of the $\pi_1\pi_1^*$ bright state of tropothione increases 0.04 eV when the radius is modified from 1.80 to 3.0 Å providing, thus, a better agreement with the full-QM result. However, this energy variation is very small in comparison with the strong red-shift underwent by the $n\pi^*$ states that go from 2.75 to 2.54 eV and from 3.68 to 3.44 eV. This red-shift induced by the increase of the S radius can be understood using the following simple model represented in Figure 6b. In the ground state, the nonbonding orbital centered at the S atom possess two electrons. These two electrons undergo attractive interactions with the positive charges of the cavity surface surrounding the S atom. When the radius of the S sphere is increased, the attractive interactions are smaller and the

ground state is energetically destabilized. In the $n\pi^*$ excited state, the n orbital possesses only one electron and the attractive interactions with the positive charges of the cavity surface are smaller. When the radius of the S sphere increases the $n\pi^*$ state also suffers an energetic destabilization, however, this energy increase is smaller than the one experienced by the ground state due to the weaker attractive interactions. Therefore, the increase of S radius results in a net red-shift of the excitation energy. Based on these results it is clear that the radius of S should be reparameterized to obtain more reliable excited-state energies from QM/PCM calculations.

The QM/MMee approach provides DOS bands in good agreement with the full-QM computations, with errors ranging from 0.00 to 0.11 eV. The QM/MMee accuracy is slightly worse than that of the best QM/PCM results for pyridine and tropone. In the case of tropothione, QM/MMee performs much better than QM/PCM if the S radius is not manually modified in the later approach. Moreover, the relative intensities from QM/MMee agree very well with the full-QM intensities for the three chromophores as shown in Figure 5. Surprisingly, the QM/MMpol approach shows the worst performance of the three classical models. The energies of the DOS bands of the three chromophores are strongly overestimated, presenting blue-shifts up to 0.26 eV. This is not expected considering that QM/MMpol described very well the absorption spectra as shown in Section 3.1. The absorption spectra of the three chromophores is mainly composed by states with strong $\pi\pi^*$ character, in which the involved orbitals are delocalized along the aromatic rings. This type of transitions is mainly affected by interactions between the chromophore and the bulk solvation, while specific interactions cause only minor energy alterations. Contrary, the $n\pi^*$ electronic states are strongly influenced by hydrogen bonding. Therefore, our results suggest that the QM/MMpol method describe properly interactions with the bulk solvent but largely overestimate hydrogen-bonding effects. Thus, further

parameterization is needed to improve the accuracy of QM/MMpol in describing $n\pi^*$ transitions in aqueous solution.

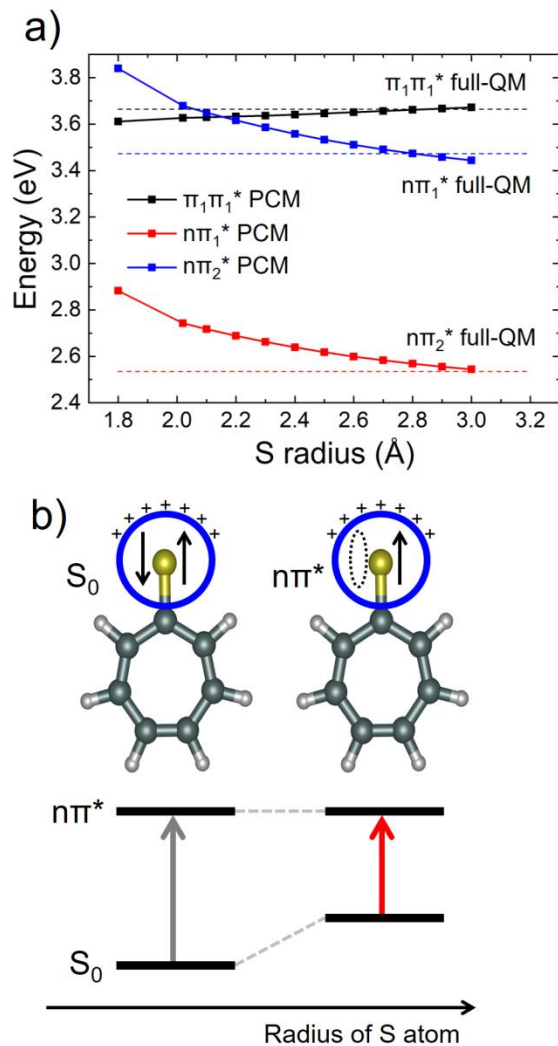


Figure 6. (a) Variation of the brightest state ($\pi_1\pi_1^*$) and the two-lowest $n\pi^*$ states ($n\pi_1^*$ and $n\pi_2^*$) of trophothione with the radius of the S atom, which is modified from 1.8 to 3.0 Å in the QM/PCM calculation. The dashed horizontal lines indicate the energies at the maxima of the full-QM bands. (b) Schematic representation of the PCM sphere for the S atom and the charges located on its surface interacting with the two electron of the n orbital in the ground state (S_0)

and with only one electron of the n orbital in the $n\pi^*$ state (up). The dashed ellipse indicates the hole created after the $n\pi^*$ excitation. Energy increase of S_0 and red-shift of the excitation energy when the radius of the S atom is increased (down).

4. CONCLUSIONS

The solvent effects on the electronically excited states of the chromophores pyridine, tropone and trophione in aqueous solution have been analyzed employing three QM/classical schemes, namely, QM/PCM, QM/MMee and QM/MMpol. The absorption spectra and the $n\pi^*$ DOS calculated with the classical approaches were compared with excited-state computations carried out using a more accurate model, in which a large number of water molecules was described at the same level of theory as the chromophore.

The electronic transitions that mostly contribute to the absorption spectrum of the three chromophores are $\pi\pi^*$ transitions. Our calculations have shown that interactions between the chromophore and the bulk solvent induce important energy shifts in the absorbing states, most of which can be explained by using a simple electrostatic model that only considers the relationship between the excited- and ground-state dipole moments.

One of the $\pi\pi^*$ absorption bands of pyridine shows red-shift upon solvation induced by hydrogen bonding with one water molecule. Remarkably, in general, the QM/PCM approach provided the most accurate results attending to excitation energies, including that of the absorption band of pyridine that presents important hydrogen-bonding effects. The QM/MMpol scheme performs very similarly as QM/PCM and better than QM/MMee, showing that the description of the

mutual polarization between the chromophore and the solvent improves the quality of the excited-state energies of $\pi\pi^*$ states. Both QM/MMee and QM/MMpol reproduce better than QM/PCM the relative intensity of the absorption bands. Therefore, the inclusion of explicit solvent molecules and thermal sampling is important to obtain accurate intensities.

Hydrogen bonding induces a strong blue-shift in the $n\pi^*$ DOS of the systems investigated. QM/PCM provided the most accurate energies for pyridine and tropone, but it presented very large errors for tropothione, whose hydrogen-bonded atom is S. However, the results significantly improve when the radius of S was increased to 3 Å, providing then the smallest errors among the three classical approaches. This shows that the parameterization of the S atom in PCM is not as good as that of the O and N atoms. The QM/MMee excitation energies for the three chromophores are reasonably accurate but slightly worse than the QM/PCM ones when the radius of S is modified. Unexpectedly, despite producing accurate energies for the $\pi\pi^*$ states, the QM/MMpol approach failed to reproduce hydrogen bonding effects on the $n\pi^*$ states in comparison with the other two classical approaches. Specifically, the hydrogen-bond-induced blue-shift was overestimated by QM/MMpol.

Overall, it is notable that the continuum model was able to reproduce very well not only the interactions between the chromophore and bulk solvent but also hydrogen-bonding effects. The use of explicit models is thus not required for describing the effect of hydrogen bonding on excited-state energies as it is usually stated in the literature. This is a comforting conclusion since QM/PCM calculations do not require sampling of the solvent degrees of freedom followed by hundreds of excited-state calculations, as QM/MM schemes do, but it only requires a geometry optimization followed by a single excited-state calculation. However, this conclusion is valid so far for vertical-energy calculations. More complex situations, e.g., excited-state dynamics, will

likely demand the use of explicit solvent, although the good performance of continuum models cannot be a priori ruled out.

ACKNOWLEDGMENTS

LG wants to thank her mentors, Otilia Mó and Manuel Yáñez, for introducing her to the field of quantum chemistry and the world of hydrogen bonds. Without their enthusiasm for science and their continuous support her academic life would have been surely different. LG and JJN further acknowledge the University of Vienna for financial support, while MDV and MFSJM thank the Marie Curie Actions, within the Innovative Training Network-European Joint Doctorate in Theoretical Chemistry and Computational Modelling TCCM-ITN-EJD-642294, for their respective PhD grants. We also thank Benedetta Mennucci for making the QM/MMpol code available and the VSC for generous allocation of computer time. The QM/MMpol calculations have been run in the computer cluster of the Molecolab of the University of Pisa.

REFERENCES

- (1) Marquetand, P.; Nogueira, J. J.; Mai, S.; Plasser, F.; González, L. *Molecules* **2017**, *22*, 49.
- (2) González, L.; Escudero, D.; Serrano-Andrés, L. *ChemPhysChem* **2012**, *13*, 28.
- (3) Nogueira, J. J.; González, L. *Annu. Rev. Phys. Chem.* **2018**, in press.
- (4) Szabla, R.; Šponer, J.; Góra, R. W. *J. Phys. Chem. Lett.* **2015**, *6*, 1467.
- (5) Nogueira, J. J.; Corani, A.; El Nahhas, A.; Pezzella, A.; d'Ischia, M.; González, L.; Sundström, V. *J. Phys. Chem. Lett.* **2017**, *8*, 1004.
- (6) Barbatti, M. *J. Am. Chem. Soc.* **2014**, *136*, 10246.
- (7) Szabla, R.; Kruse, H.; Šponer, J.; Góra, R. W. *Phys. Chem. Chem. Phys.* **2017**, *19*, 17531.
- (8) Nogueira, J. J.; Meixner, M.; Bittermann, M.; González, L. *ChemPhotoChem* **2017**, *1*, 178.
- (9) Nogueira, J. J.; Oppel, M.; González, L. *Angew. Chem. Int. Ed.* **2015**, *54*, 4375.
- (10) Dumont, E.; Wibowo, M.; Roca-Sanjuán, D.; Garavelli, M.; Assfeld, X.; Monari, A. *J. Phys. Chem. Lett.* **2015**, *6*, 576.
- (11) Daday, C.; Curutchet, C.; Sinicropi, A.; Mennucci, B.; Filippi, C. *J. Chem. Theory Comput.* **2015**, *11*, 4825.
- (12) Cramer, C. J.; Truhlar, D. G. *Chem. Rev.* **1999**, *99*, 2161.
- (13) Orozco, M.; Luque, F. J. *Chem. Rev.* **2000**, *100*, 4187.
- (14) Tomasi, J.; Mennucci, B.; Cammi, R. *Chem. Rev.* **2005**, *105*, 2999.

- (15) Tomasi, J.; Persico, M. *Chem. Rev.* **1994**, *94*, 2027.
- (16) Mennucci, B. *WIREs Comput. Mol. Sci.* **2012**, *2*, 386.
- (17) Klamt, A. *WIREs Comput. Mol. Sci.* **2011**, *1*, 699.
- (18) Thompson, J. D.; Cramer, C. J.; Truhlar, D. G. *J. Phys. Chem. A* **2004**, *108*, 6532.
- (19) Wong, M. W.; Frisch, M. J.; Wiberg, K. B. *J. Am. Chem. Soc.* **1991**, *113*, 4776.
- (20) Cammi, R.; Cappelli, C.; Mennucci, B.; Tomasi, J. Properties of Excited States of Molecules in Solution Described with Continuum Solvation Models. In *Practical Aspects of Computational Chemistry*; Springer: Dordrecht, 2009.
- (21) Senn, H. M.; Thiel, W. *Angew. Chem. Int. Ed.* **2009**, *48*, 1198.
- (22) Brunk, E.; Rothlisberger, U. *Chem. Rev.* **2015**, *115*, 6217.
- (23) Curutchet, C.; Muñoz-Losa, A.; Monti, S.; Kongsted, J.; Scholes, G. D.; Mennucci, B. *J. Chem. Theory Comput.* **2009**, *5*, 1838.
- (24) Caricato, M.; Lipparini, F.; Scalmani, G.; Cappelli, C.; Barone, V. *J. Chem. Theory Comput.* **2013**, *9*, 3035.
- (25) Mewes, J.-M.; Herbert, J. M.; Dreuw, A. *Phys. Chem. Chem. Phys.* **2017**, *19*, 1644.
- (26) Sato, H. Electronic Structure and Chemical Reaction in Solution. In *Molecular Theory of Solvation. Understanding Chemical Reactivity*; Hirata, F., Ed.; Springer: Dordrecht, 2004; Vol. 24.
- (27) Sinnecker, S.; Neese, F. Theoretical Bioinorganic Spectroscopy. In *Atomistic Approaches in Modern Biology. Topics in Current Chemistry*; Reiher, M., Ed.; Springer: Berlin, Heidelberg, 2006; Vol. 268.
- (28) Orozco, M.; Marchán, I.; Soteras, I.; Vreven, T.; Morokuma, K.; Mikkelsen, K. V.; Milani, A.; Tommasini, M.; Zoppo, M. D.; Castiglioni, C.; Aguilar, M. A.; Sánchez, M. L.; Martín, M. E.; Galván, I. F.; Sato, H. Beyond the Continuum Approach. In *Continuum Solvation Models in Chemical Physics: From Theory to Applications*; Mennucci, B., Cammi, R., Eds.; John Wiley & Sons, Ltd: Chichester, 2007.
- (29) Tomasi, J.; Cancès, E.; Pomelli, C. S.; Caricato, M.; Scalmani, G.; Frisch, M. J.; Cammi, R.; Basilevsky, M. V.; Chuev, G. N.; Mennucci, B. Modern Theories of Continuum Models. In *Continuum Solvation Models in Chemical Physics: From Theory to Applications (eds B. Mennucci and R. Cammi)*; John Wiley & Sons: Chichester, UK, 2007; pp 1.
- (30) Umeyama, H.; Morokuma, K. *J. Am. Chem. Soc.* **1977**, *99*, 1316.
- (31) Frisch, M. J.; Trucks, G. W.; Schlegel, H. B.; Scuseria, G. E.; Robb, M. A.; Cheeseman, J. R.; Scalmani, G.; Barone, V.; Mennucci, B.; Petersson, G. A.; Nakatsuji, H.; Caricato, M.; Li, X.; Hratchian, H. P.; Izmaylov, A. F.; Bloino, J.; Zheng, G.; Sonnenberg, J. L.; Hada, M.; Ehara, M.; Toyota, K.; Fukuda, R.; Hasegawa, J.; Ishida, M.; Nakajima, T.; Honda, Y.; Kitao, O.; Nakai, H.; Vreven, T.; Montgomery, J. A., Jr.; ; Peralta, J. E.; Ogliaro, F.; Bearpark, M.; Heyd, J. J.; Brothers, E.; Kudin, K. N.; Staroverov, V. N.; Kobayashi, R.; Normand, J.; Raghavachari, K.; Rendell, A.; Burant, J. C.; Iyengar, S. S.; Tomasi, J.; Cossi, M.; Rega, N.; Millam, N. J.; Klene, M.; Knox, J. E.; Cross, J. B.; Bakken, V.; Adamo, C.; Jaramillo, J.; Gomperts, R.; Stratmann, R. E.; Yazyev, O.; Austin, A. J.; Cammi, R.; Pomelli, C.; Ochterski, J. W.; Martin, R. L.; Morokuma, K.; Zakrzewski, V. G.; Voth, G. A.; Salvador, P.; Dannenberg, J. J.; Dapprich, S.; Daniels, A. D.; Farkas, Ö.; Foresman, J. B.; Ortiz, J. V.; Cioslowski, J.; Fox, D. J. *Gaussian 09*, Revision D.01; Gaussian, Inc.: Wallingford CT, 2013.
- (32) Yanai, T.; Tew, D. P.; Handy, N. C. *Chem. Phys. Lett.* **2004**, *393*, 51.
- (33) Cossi, M.; Barone, V. *J. Chem. Phys.* **2001**, *115*, 4708.
- (34) Impropa, R.; Barone, V. *J. Mol. Struct. THEOCHEM* **2009**, *914*, 87.

- (35) Case, D. A.; Cerutti, D. S.; Cheatham III, T. E.; Darden, T. A.; Duke, R. E.; Giese, T. J.; Gohlke, H.; Goetz, A. W.; Greene, D.; Homeyer, N.; Izadi, S.; Kovalenko, A.; Lee, T. S.; LeGrand, S.; Li, P.; Lin, C.; Liu, J.; Luchko, T.; Luo, R.; Mermelstein, D.; Merz, K. M.; Monard, G.; Nguyen, H.; Omelyan, I.; Onufriev, A.; Pan, F.; Qi, R.; Roe, D. R.; Roitberg, A.; Sagui, C.; Simmerling, C. L.; Botello-Smith, W. M.; Swails, J.; Walker, R. C.; Wang, J.; Wolf, R. M.; Wu, X.; Xiao, L.; York, D. M.; Kollman, P. A. AMBER 17 University of California, San Francisco, 2017.
- (36) Crowley, M. F.; Darden, T. A.; Cheatham III, T. E.; Deerfield II, D. W. *J. Supercomput.* **1997**, *11*, 255.
- (37) Miyamoto, S.; Kollman, P. A. *J. Comput. Chem.* **1992**, *13*, 952.
- (38) Wang, J.; Wolf, R. M.; Caldwell, J. W.; Kollman, P. A.; Case, D. A. *J. Comput. Chem.* **2004**, *25*, 1157.
- (39) Jorgensen, W. L.; Chandrasekhar, J.; Madura, J. D.; Impey, R. W.; Klein, M. L. *J. Chem. Phys.* **1983**, *79*, 926.
- (40) Caprasecca, S.; Jurinovich, S.; Viani, L.; Curutchet, C.; Mennucci, B. *J. Chem. Theory Comput.* **2014**, *10*, 1588.
- (41) Wang, J.; Cieplak, P.; Li, J.; Hou, T.; Luo, R.; Duan, Y. *J. Phys. Chem. B* **2011**, *115*, 3091.
- (42) Wang, J.; Cieplak, P.; Li, J.; Cai, Q.; Hsieh, M.; Lei, H.; Luo, R.; Duan, Y. *J. Phys. Chem. B* **2011**, *115*, 3100.
- (43) Jurinovich, S.; Curutchet, C.; Mennucci, B. *ChemPhysChem* **2014**, *15*, 3194.
- (44) Plasser, F.; Lischka, H. *J. Chem. Theory Comput.* **2012**, *8*, 2777.
- (45) Plasser, F.; Wormit, M.; Dreuw, A. *J. Chem. Phys.* **2014**, *141*.
- (46) Plasser, F. TheoDORE 1.5.1: a package for theoretical density, orbital relaxation, and exciton analysis, available from <http://theodore-qc.sourceforge.net>
- (47) Roe, D. R.; Cheatham, T. E. *J. Chem. Theory Comput.* **2013**, *9*, 3084.
- (48) Dreuw, A.; Head-Gordon, M. *Chem. Rev.* **2005**, *105*, 4009.

Table of Contents Figure.

